CeIr_{3}Ge_{7}: A local moment antiferromagnetic metal with extremely low ordering temperature

Binod K. Rai, Jacintha Banda, Macy Stavinoha, R. Borth, D.-J. Jang, Katherine A. Benavides, D. A. Sokolov, Julia Y. Chan, M. Nicklas, Manuel Brando, C.-L. Huang, and E. Morosan

Phys. Rev. B **98**, 195119 — Published 16 November 2018

DOI: 10.1103/PhysRevB.98.195119

$CeIr_3Ge_7$: a local moment antiferromagnetic metal with extremely low ordering temperature

Binod K. Rai[1], Jacintha Banda[2], Macy Stavinoha[3], R. Borth[2], D.-J. Jang[2], Katherine A. Benavides[4], D. A. Sokolov[2], Julia Y. Chan[4], M. Nicklas[2], Manuel Brando[2], C.-L. Huang[1], and E. Morosan[1]

[1] *Department of Physics and Astronomy, Rice University, Houston, TX 77005 USA*

[2] *Max Planck Institute for Chemical Physics of Solids, Dresden, 01187 Germany*

[3] *Department of Chemistry, Rice University, Houston, TX 77005 USA*

[4] *Department of Chemistry & Biochemistry, University of Texas at Dallas, Richardson, TX 75080 USA*

(Dated: July 30, 2018)

$CeIr_3Ge_7$ is an antiferromagnetic metal with a remarkably low ordering temperature $T_N = 0.63$ K, while most Ce-based magnets order between 2 and 15 K. Thermodynamic and transport properties as a function of magnetic field or pressure do not show signatures of Kondo correlations, interaction competition, or frustration, as had been observed in a few antiferromagnets with comparably low or lower T_N. The averaged Weiss temperature measured below 10 K is comparable to T_N suggesting that the RKKY exchange coupling is very weak in this material. The unusually low T_N in $CeIr_3Ge_7$ can therefore be attributed to the large Ce-Ce bond length of about 5.7 Å, which is about 1.5 Å larger than in the most Ce-based intermetallic systems.

I. INTRODUCTION

Compounds containing Ce or Yb ions have been studied extensively due to their diverse ground states originating from the competition between several energy scales. The competition between Ruderman-Kittel-Kasuya-Yosida (RKKY) exchange interaction and Kondo coupling gives rise to intermediate valence behavior[1–4] or Kondo screening[4–9] which, in turn, often result in unconventional superconductivity, non-Fermi liquid behavior, and quantum criticality[7,10–13]. If the hybridization between f electrons and conduction electrons is very weak, the ground states of these systems are dictated by RKKY exchange interaction and crystal electric field (CEF) effects, resulting in long-range magnetic order.[14–16] In the case of the Ce local moment metals without the Kondo effect, the ordering temperatures range from $T_C = 115$ K[17,18] in ferromagnetic $CeRh_3B_2$, to $T_C = 0.44$ K[19,20] in ferromagnetic $Ce_3Pt_{23}Si_{11}$, while much lower temperatures can be expected for the Yb analogues[21]. Lower ordering temperatures in both Ce^{3+} and Yb^{3+} compounds could occur from any combination of effects including Kondo, competition between different exchange interactions, strong CEF anisotropy, or large distances between rare-earth ions (d_{R-R}) that minimize the RKKY exchange coupling J_{RKKY}. Compounds with low ordering temperatures often involve either weaker-than-RKKY exchange, as is the case in insulators, or multipolar order[22], in which case the resulting order is almost always underlined by heavy fermion (HF) behavior. Remarkably low Néel temperatures were also found in some intermetallic cage compounds having also large d_{R-R}, such as $T_N = 0.18$ K in $Ce_4Pt_{12}Sn_{25}$[23] and $T_N = 0.89$ K in $CePt_4Ge_{12-x}Sb_x$[24]. However, the low ordering temperatures have been attributed to either the onset of Kondo screening or frustration.

Here we report the discovery of $CeIr_3Ge_7$, a new intermetallic compound without Kondo effect and no geometric frustration, with a remarkably low antiferromagnetic (AFM) ordering temperature $T_N = 0.63$ K. This is one of several R = Ce or Yb compounds we recently discovered in the RT_3M_7 (1-3-7) class of compounds with T = transition metal and M = group 14 element[9,25], a family of rhombohedral intermetallics with the $ScRh_3Si_7$ structure type[26,27]. The R sublattice forms a distorted cubic structure, with nearest-neighbor d_{R-R} around 5.7 Å. Strong electron correlations in the Yb members of this family result in HF behavior and ferromagnetic or AFM ordering at temperatures as high as 7.5 K. Remarkably, $CeIr_3Ge_7$ is weakly correlated, and even with similar d_{R-R}, the ordering temperature is much smaller than in the Yb analogues ($T_N = 7.5$ K in $YbRh_3Si_7$[9], $T_C = 2.4$ K in $YbIr_3Ge_7$[25], $T_N = 4$ K in $YbIr_3Si_7$[28]). No frustration is present in $CeIr_3Ge_7$, as the Weiss temperature in the limit of absolute zero is close to T_N. This system is a good metal, with residual resistivity values $\rho_0 \sim 20\ \mu\Omega$ cm and a residual resistivity ratio RRR = $\rho(300K)/\rho_0 \sim 5$. No Kondo correlations are apparent as most of the magnetic entropy is released below T_N. In the absence of Kondo effect or frustration, the low T_N in $CeIr_3Ge_7$ is attributed to the large distance d_{R-R}. This points to the potential of the 1-3-7 family to reveal Ce or Yb compounds with low ordering temperatures, which, in turn, may be easily tuned towards absolute zero transitions and quantum critical regimes. Furthermore, an added appeal for Ce- or Yb-based metals with low magnetic exchange is their potential for demagnetization cooling below 2 K. These metallic magnets are preferable to the commonly used paramagnetic salts, which are insulators, or ^{3}He-systems, which are expensive. Our recent discovery of $YbPt_2Sn$[29], a metallic system with weak exchange coupling and $T_N \sim 0.25$ K, similar to $CeIr_3Ge_7$, reinforces the potential of our low temperature magnet for cooling applications.

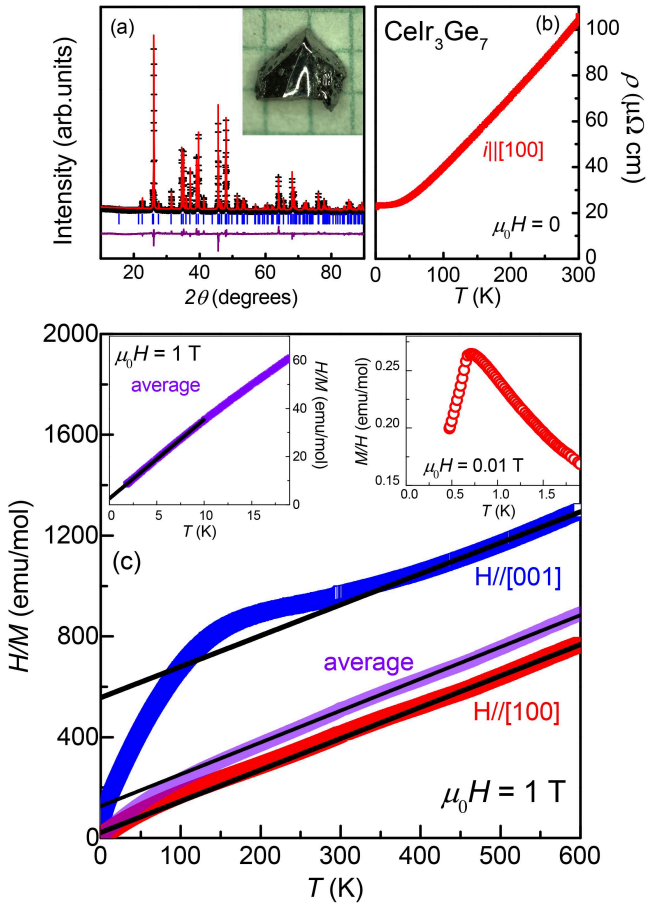

FIG. 1: (a) Room temperature (symbols) and calculated (red line) powder x-ray diffraction patterns of $CeIr_3Ge_7$, together with the expected peak positions (blue vertical lines) for space group $R\bar{3}c$ and lattice parameters a = 7.8915(8) Å and c = 20.788(6) Å. Violet curve is the difference between data and calculated patterns. Inset: crystal picture on millimeter-scaled paper. (b) Zero-field resistivity with current parallel to the [100] axis. (c) Inverse magnetic susceptibility H/M vs. T for magnetic field H||[001] (blue), [100] (red), and a polycrystalline average (violet). Solid lines are high temperature Curie-Weiss fits, with Weiss temperatures of −360 K, −20 K, and −100 K for H||[001], [100], and the polycrystalline average, respectively (see text). Left inset: the low-temperature H/M vs. T with a linear fit for the polycrystalline average. Right inset: the low-temperature M/H vs. T for H||[100].

II. EXPERIMENTAL METHODS

Temperature-dependent AC resistivity was measured using a Quantum Design (QD) physical properties measurement system (PPMS) with a ^{3}He insert using I = 2 mA and f = 622.2 Hz. DC magnetic susceptibility measurements were performed on a QD magnetic properties measurement system equipped with an iHelium ^{3}He attachment. Specific heat measurements at ambient pressure were collected using a thermal-relaxation method in QD PPMS with a ^{3}He insert for the oriented crystal. An unoriented crystal was used for the specific heat measurement down to 0.1 K in a QD PPMS DynaCool system with a dilution refrigeration insert. Specific heat measurements under pressure were performed using a compensated heat-pulse method[30]. The sample was put into a Teflon capsule together with a piece of Pb whose superconducting transition temperature as a function of pressure served as a manometer. The capsule was mounted in a clamped-type CuBe cell using Fluorinert (3M) as a pressure transmitting medium. The background specific heat of the empty cell was determined in separate runs and was subtracted from the raw data to obtain the sample's contribution.

III. ANALYSIS AND DISCUSSION

$CeIr_3Ge_7$ crystallizes in the $R\bar{3}c$ rhombohedral $ScRh_3Si_7$ structure type[26,27]. The very few 1-3-7 compounds known so far are RAu_3Ga_7 (R = Gd-Yb)[31,32], non-magnetic RAu_3Al_7 (R = Ce-Sm, Gd-Lu)[33], and magnetic $Eu(Rh,Ir)_3Ge_7$[34]. Recently we discovered the first magnetic Ce and Yb 1-3-7 compounds. All of the newly discovered compounds were synthesized in single crystal form using a self-flux growth method[35,36], with details described elsewhere[9]. Single crystal x-ray diffraction measurements confirm the $ScRh_3Si_7$ structure type and verify the purity and stoichiometry of these compounds. The details of the x-ray diffraction and experimental methods are described in the Appendix and the crystallographic parameters are summarized in Table I. A nonmagnetic analogue YIr_3Ge_7 polycrystalline sample was prepared by arc melting. Figure 1(a) shows a powder x-ray pattern and structural refinement for $CeIr_3Ge_7$ with a photo of a crystal shown in the inset. In this rhombohedral crystal structure, the R atoms form a distorted cubic sublattice[9], with the body diagonal of the cuboid parallel to the c axis of the equivalent hexagonal unit cell. Notably, the distances $d_{R-R} \sim 5.7$ Å are larger than in many magnetic R intermetallics, but do not change significantly for R = Ce or Yb in the 1-3-7 structure. This observation becomes most relevant when trying to explain the low ordering temperature $T_N = 0.63$ K in $CeIr_3Ge_7$. Several scenarios may in principle result in low T_N in Ce compounds, such as the Kondo effect, frustration or exchange coupling competition, weak exchange due to large d_{Ce-Ce}. The following discussion is based on evidence against most, if not all, of these scenarios in $CeIr_3Ge_7$, rendering this compound a unique non-Kondo metal with extremely low ordering temperature.

The $\mu_0 H = 0$ resistivity measurements (Fig. 1(b)) show that $CeIr_3Ge_7$ is a good metal, with a RRR = 5 and residual resistivity $\rho_0 \sim 20$ $\mu\Omega$cm. However, upon cooling from room temperature, the resistivity is linear in temperature, and no signatures of Kondo correlations are apparent. The lack of Kondo effect will be further corroborated by the specific heat data shown later. For now, we turn to the magnetic susceptibility measured along

($H\|[001]$) and perpendicular ($H\|[100]$) to the c axis of the equivalent hexagonal unit cell. The inverse susceptibility H/M (Fig. 1(c)), measured up to 600 K, reveals large easy-plane CEF anisotropy. The average susceptibility is calculated as $M_{ave} = (M_{001} + 2M_{100})/3$. Fits to the Curie-Weiss law at high temperatures are shown in solid black lines. The experimental effective moment μ_{eff}^{exp} extracted from the fit of the average susceptibility (violet, Fig. 1(c)) is $\mu_{eff}^{exp} = 2.52\ \mu_B/Ce^{3+}$, pointing to fully trivalent Ce ions in $CeIr_3Ge_7$, since the calculated Ce^{3+} effective moment $\mu_{eff}^{calc} = 2.52\ \mu_B/Ce^{3+}$ is virtually identical to the experimental value. The negative Weiss temperatures indicate AFM correlations. The H/M data deviate from the Curie-Weiss law due to CEF splitting of the $J = 5/2$ multiplet. The deviation indicates a separation of the first excited CEF doublet of ~ 400 K, consistent with the CEF calculations which will be reported elsewhere[37].

In the $T \to 0$ limit, the inverse susceptibility intercept with the temperature axis is around -2 K for M_{ave} (left inset, Fig. 1(c)), comparable to the low ordering temperature $T_N \sim 0.6$ K indicated by the cusp in M/H vs. T for $H\|[001]$ (right inset, Fig. 1(c)). These observations can be reconciled by considering the Weiss temperatures at $T \to 0$ to reflect the exchange coupling J_{ex}, which consequently indicates that J_{ex} is inherently small in $CeIr_3Ge_7$. We show the $M(H)$ isotherms in Fig. 2 for $H\|[100]$ (red symbols) and $H\|[001]$ (blue symbols), in the ordered state $T = 0.5$ K (full symbols) and the paramagnetic state $T = 1.8$ K (open symbols). The magnetization data agrees with the CEF calculations with an exchange interaction of 2.4 K[37]. The $M(H)$ measurements confirm the in-plane and out-of-plane magnetic anisotropies, and, more quantitatively, are in good agreement with the calculated moments of 0.91 μ_B/Ce and 0.33 μ_B/Ce along the easy ([100]) and hard ([001]) directions, respectively[37]. A magnetic field close to $\mu_0 H = 1.7$ T is required for saturation in the easy direction (squares, Fig. 2), while a linear extrapolation of $M(H \parallel [001])$ suggests a magnetic field in excess of 20 T is needed to reach saturation in the hard direction.

Because of this extremely large anisotropy, and the large magnetic field scale in the hard ([001]) direction, we focus next only on the field dependence of the ordering temperature T_N for the easy direction $H\|[100]$, as illustrated by the M/H and specific heat C_p data in Fig. 3. For AFM systems, a peak in C_p at T_N is expected to correspond to a peak in $d(MT)/dT$[38], and this is illustrated for $\mu_0 H = 0.01$ T (solid line, right axis) in Fig. 3(a). Both ambient pressure M/H and C_p measurements (3(a-b)) reveal the expected suppression of T_N with increasing H, such that above $\mu_0 H = 1.7$ T, no peak can be resolved above 350 mK. Consistent with the zero field resistivity data in Fig. 1(b), the specific heat data show an entropy release of $\sim 2/3$ Rln2 at T_N (solid line, right axis in Fig. 3d), reaffirming the absence of both Kondo effect and strong correlations in $CeIr_3Ge_7$. To further rule out the presence of Kondo screening, one can consider the analysis by de Jongh and Miedema[39], which shows that an entropy release of 15%-40% of Rln2 above T_N can be expected in AFM systems around and above T_N due to the short-range magnetic interactions. Indeed this is reflected in the $H = 0$ magnetic entropy plot of $CeIr_3Ge_7$ in Fig. 3(d) (black line). Furthermore, the same model indicates that the C_p contribution from Kondo is much weaker than that from classical intersite fluctuations. Within a Heisenberg model, one expects that, far above T_N, the leading term in $C_p(T)$ is proportional to $1/T^2$, *i.e.*, $C_p/T \sim 1/T^3$. Upon applying a magnetic field (Fig. 3(b)), the dispersion of the magnons changes. In an AFM system the energy gap at Q = 0 decreases and disappears at $\mu_0 H = \mu_0 H_c \approx 1.7$ T. This results in a large increase of the low energy magnon-like excitations, which, in turn, shows up as a strong increase of C_p near and above T_N. For $H > H_c$ (full right triangles, Fig. 3(b)), a gap reopens in the magnon excitation spectra, and the specific heat evolves towards a broad anomaly related to the dominant Zeeman splitting.

Complementary to the field dependence, the pressure dependence of the specific heat (Fig. 3(c)) underlines the conclusion of small or negligible Kondo correlations: T_N increases linearly with pressures up to 1.6 GPa at a rate of $dT_N/dp = 3.71 \times 10^{-2}$ K/GPa. The increase of T_N under pressure, if only being ascribed to a volume effect, can be understood in the framework of the Doniach phase diagram[40]. The positive, yet very small, slope of $T_N(p)$ for $CeIr_3Ge_7$ suggests that this compound is located at far left of $T_N^{max}(J_{ex})$ in the Doniach diagram. The $T - H$ phase diagram in Fig. 4(a) summarizes the T_N dependence on field at ambient pressure.

Among non-Kondo magnetic Ce compounds, $CeIr_3Ge_7$ stands out (red in Fig. 4(b)) together with $CeRh_3B_2$ and $Ce_3Pt_{23}Si_{11}$. $CeRh_3B_2$ orders ferromagnetically with a remarkably large $T_C \sim 115$ K due to the enhancement

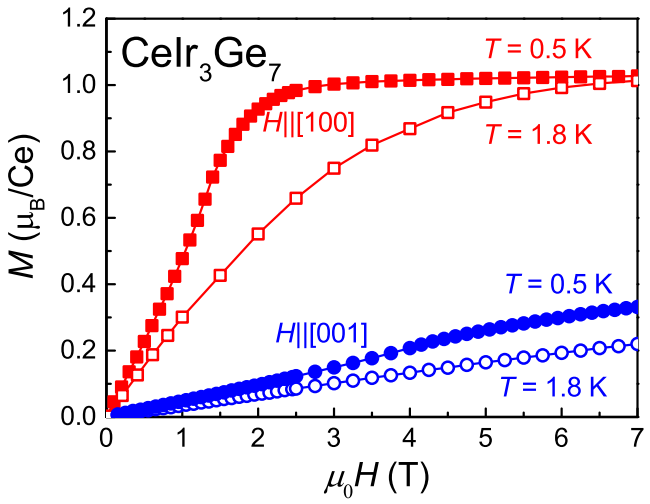

FIG. 2: $CeIr_3Ge_7$ M vs. H isotherms for $T = 0.5$ K (full symbols) and 1.8 K (open symbols) for $H\|[001]$ (blue circles) and $H\|[100]$ (red squares).

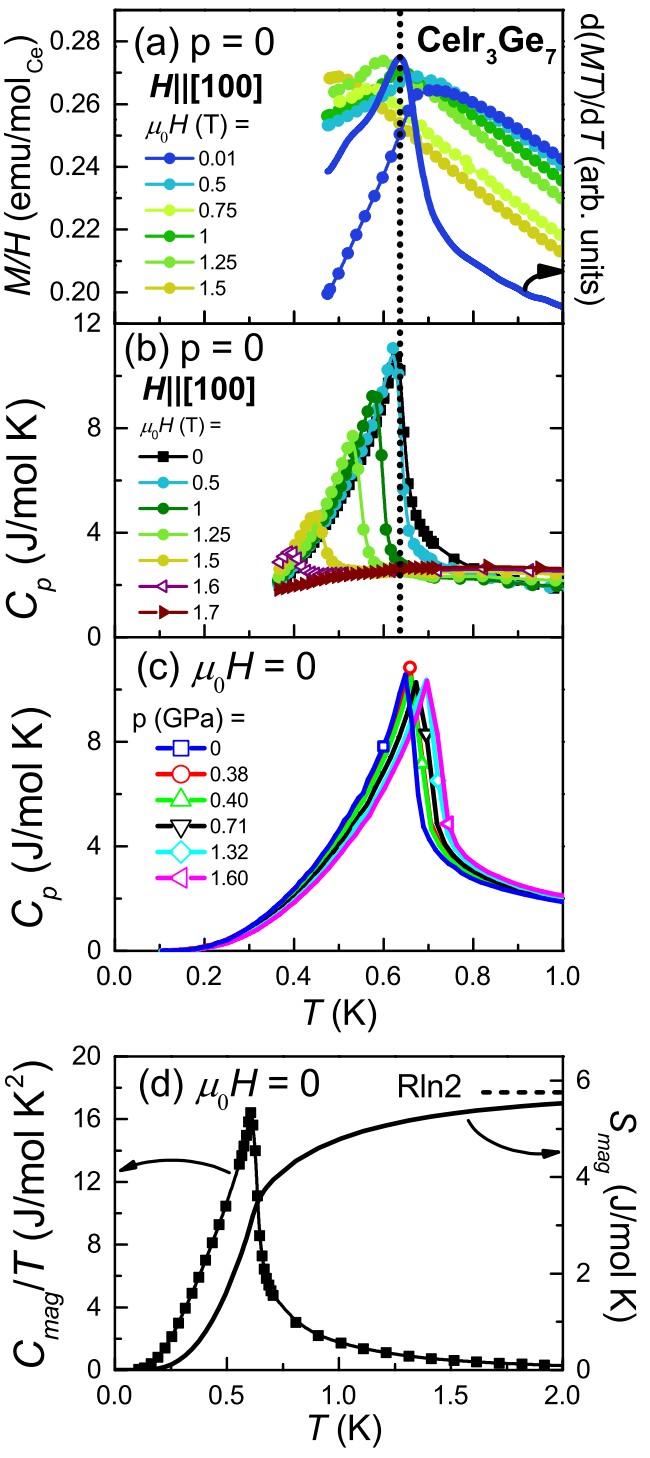

FIG. 3: (a) Left axis: magnetic susceptibility M/H *vs.* T. Right axis: d(MT)/dT*vs.*T (solid line) for $\mu_0 H = 0.01$ T. (b) Left axis: specific heat C_p *vs.* T (symbols) for different magnetic fields. The vertical dashed line through (a) to (b) marks T_N at zero field. (c) Temperature dependent specific heat for different pressures. (d) Left axis: magnetic contribution to the specific heat C_{mag}/T *vs.* T. Right axis: magnetic entropy S_{mag} *vs.* T. $C_{mag}/T = C_p/T(CeIr_3Ge_7)$ - $C_p/T(YIr_3Ge_7)$, where YIr_3Ge_7 is a nonmagnetic analogue.

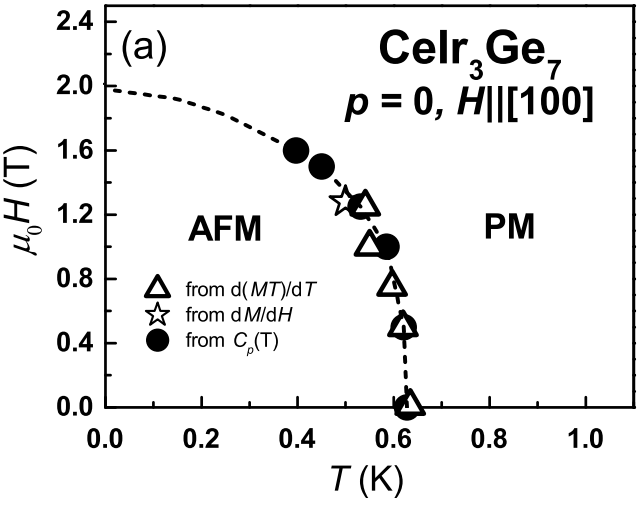

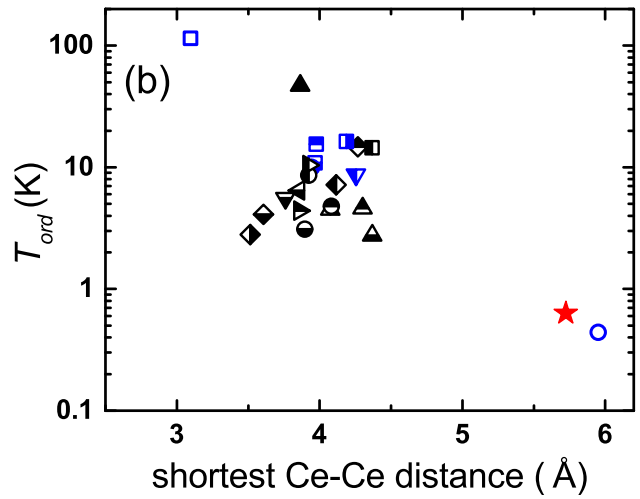

FIG. 4: (a) $T-H$ phase diagram of $CeIr_3Ge_7$ at ambient pressure with $H\|[100]$. (b) Non-Kondo Ce compounds showing their ordering temperatures with respect to the shortest Ce-Ce bond distances[17–20,41–61]. Blue symbols represent ferromagnetic (FM) ordering temperatures, black symbols represent AFM ordering temperatures, and the red star indicates $CeIr_3Ge_7$. The legend for the symbols is given in the Appendix in Table II.

of the exchange interaction from the $J = 7/2$ multiplet, despite short $d_{Ce-Ce} = 3.096$ Å[18]. On the contrary, $Ce_3Pt_{23}Si_{11}$ orders ferromagnetically with an extraordinarily low $T_C \sim 0.44$ K due to large $d_{Ce-Ce} = 5.95$ Å.[19,20] Of note is the compound $Ce_4Pt_{12}Sn_{25}$ (Ref. 23), which appears to have a record low $T_N = 0.18$ K and represents a Kondo lattice in the small exchange limit of the Doniach phase diagram. In this case, however, the extremely low T_N is a result of the large $d_{Ce-Ce} \sim 6.14$ Å, weak Kondo screening just above T_N (marked by a tail in the magnetic specific heat peak just above the ordering), and weak geometric frustration due to the three-fold point symmetry of the Ce site[62]. Except for the large $d_{Ce-Ce} \sim 5.7$ Å, none of these effects are at play in $CeIr_3Ge_7$: the low temperature Weiss temperatures (Fig.

1(c) inset) are comparable with T_N, ruling out significant frustration effects; the specific heat peak (Fig. 3(b)) terminates abruptly at T_N, and $\rho(T)$ decreases linearly with temperature before it levels off at ρ_0 at the lowest temperatures (Fig. 1(b)), therefore no Kondo screening signatures are apparent. To put $CeIr_3Ge_7$ into perspective, we summarize the non-Kondo Ce-based intermetallic compounds and plot their ordering temperatures vs. d_{Ce-Ce} in Fig. 4(b). In these compounds, the magnetism is dictated by the RKKY interactions, where the exchange interaction J is an oscillatory function of the product of the Fermi wavevector k_F and d_{Ce-Ce}, and the ordering temperature is proportional to J^2. Since the k_F is not well defined for non-spherical Fermi surfaces of those compounds, we disregard it in the comparison shown in Fig. 4(b). Qualitatively, the order temperatures scale with d_{Ce-Ce}: the larger (smaller) the d_{Ce-Ce}, the smaller (larger) ordering temperature. Ce and Yb magnetic (trivalent) compounds are often thought as electron-hole analogues. In metals, due to deeper localization of the $4f$ electron and the larger strength of the spin-orbit coupling in the latter[21], smaller ordering temperatures are often expected in the latter compared to the former. What we find is that $YbIr_3Ge_7$ is in fact an HF ferromagnet with $T_C \sim 2.4$ K, despite the nearly identical d_{R-R} in both the Ce and Yb analogues.[25] This may reflect that the details of the band structure near the Fermi surface of Ce and Yb analogues play an important role with regards to magnetism.

IV. CONCLUSIONS

In summary, $CeIr_3Ge_7$ in particular and more generally the 1-3-7 family of magnetic compounds provide a fertile ground for exploring magnetic correlations and the competition among various energy scales (RKKY, Kondo, CEF) which could result in novel quantum critical regimes. In addition, their rhombohedral structure allows for very weak coupling between the Ce atoms in a good metallic environment, similar to what was observed in $YbPt_2Sn$[29]. This is an excellent precondition for metallic magnets that can be used for adiabatic demagnetization cooling below 2 K, instead of insulating paramagnetic salts.

Acknowledgements

We thank J. Simone, J. D. Thompson, C. Geibel, and W. Hu for fruitful discussions. Work at Rice University was supported by the Gordon and Betty Moore Foundation EPiQS Initiative through grant GBMF 4417. The work at University of Texas at Dallas was supported by NSF-DMR 1700030. BR acknowledges partial support from a QuantEmX grant from ICAM. EM acknowledges travel support to Max Planck Institute in Dresden, Germany from the Alexander von Humboldt Foundation Fellowship for Experienced Researchers.

[1] R. Currat, R. G. Lloyd, P. W. Mitchell, A. P. Murani, and J. W. Ross, *Physica B* **156**, 812 (1989).
[2] T. Mazet, D. Malterre, M. Francois, C. Dallera, M. Grioni, and G. Monaco, *Phys. Rev. Lett.*, **111** 096402 (2013).
[3] Binod K. Rai and E. Morosan, *APL Mater.* **03** 041511 (2015).
[4] Binod K. Rai, Iain W. H. Oswald, Julia Y. Chan, and E. Morosan, *Phys. Rev. B* **93**, 035101 (2016).
[5] E. Morosan, S. L. Bud'ko, Y. A. Mozharivskyj, P. C. Canfield, *Phys. Rev. B* **73**, 174432 (2006).
[6] P. Gegenwart, T. Westerkamp, Krellner, Y. Tokiwa, S. Paschen, C. Geibel, F. Steglich, E. Abrahams, and Q. Si, *Science* **315**, 969 (2007).
[7] Johnpierre Paglione, T. A. Sayles, P.-C. Ho, J. R. Jeffries, and M. B. Maple, *Nat. Phys.* **3**, 703 (2007).
[8] Binod K. Rai, Iain W. H. Oswald, Wenjing Ban, C.-L. Huang, V. Loganathan, A. M. Hallas, M. N. Wilson, G. M. Luke, L. Harriger, Q. Huang, Y. Li, Sami Dzsaber, Julia Y. Chan, N. L. Wang, Silke Paschen, J. W. Lynn, Andriy H. Nevidomskyy, P. Dai, Q. Si, and E. Morosan, *arXiv*: 1805.01918.
[9] Binod K. Rai, S. Chikara, Xiaxin Ding, Iain W. H. Oswald, R. Schoenemann, V. Loganathan, A. M. Hallas, H. B. Cao, M. Stavinoha, Haoran Man, Scott Carr, John Singleton, Vivien Zapf, Katherine Benavides, Julia Y. Chan, Q. R. Zhang, D. Rhodes, Y. C. Chiu, Luis Balicas, A. A. Aczel, Q. Huang, Jeffrey W. Lynn, J. Gaudet, D. A. Sokolov, Pengcheng Dai, Andriy H. Nevidomskyy, C.-L. Huang, and E. Morosan, *arXiv*: 1803.04013.
[10] H. v. Löhneysen, A. Rosch, M. Vojta, and P. Wöfle, *Rev. Mod. Phys.* **79**, 1015 (2007).
[11] Erwin Schuberth, Marc Tippmann, Lucia Steinke, Stefan Lausberg, Alexander Steppke, Manuel Brando, Cornelius Krellner, Christoph Geibel, Rong Yu, Qimiao Si, and Frank Steglich, *Science* **351**, 485 (2016).
[12] J. Custers, P. Gegenwart, H. Wilhelm, K. Neumaier, Y. Tokiwa, O. Trovarelli, C. Geibel, F. Steglich, C. Pépin, and P. Coleman, *Nature* **424**, 524 (2003).
[13] Alexander Steppke, Robert Küchler, Stefan Lausberg, Edit Lengyel, Lucia Steinke, Robert Borth, Thomas Lühmann, Cornelius Krellner, Michael Nicklas, Christoph Geibel, Frank Steglich, and Manuel Brando, *Science* **339**, 933 (2013).
[14] V. Fritsch, P. Pfundstein, P. Schweiss, E. Kampert, B. Pilawa, and H. v. Löhneysen, *Phys. Rev. B* **84**, 10446 (2011).
[15] C. L. Huang, V. Fritsch, W. Kittler, and H. v. Löhneysen, *Phys. Rev. B* **86**, 214401 (2012).
[16] M. O. Ajeesh, T. Shang, W. B. Jiang, W. Xie, R. D. dos Reis, M. Smidman, C. Geibel, H. Q. Yuan, and M. Nicklas, *Scientific Report* **7**, 7338 (2017).
[17] S K Dhar, S K Malik and R Vijayaraghavan, *J. Phys. C: Solid State Phys.* **14**, L321 (1981).
[18] F Givord, J-X Boucherle, R-M Galéra, G Fillion, and P Lejay, *J. Phys.: Condens. Matter* **19**, 356208 (2007).
[19] Darshan C. Kundaliya and S. K. Malik, *Phys. Rev. B* **67**, 132411 (2003).

[20] C. Opagiste, C. Paulsen, E. Lhotel, P. Rodière, R.-M. Galera, P. Bordet, P. Lejay, *J. Magn. Magn. Mater.* **321**, 613 (2009).

[21] J. Flouquet and H. Harima *arXiv*: 0910.3110.

[22] P. Y. Portnichenko, S. Paschen, A. Prokofiev, M. Vojta, A. S. Cameron, J.-M. Mignot, A. Ivanov, and D. S. Inosov, *Phys. Rev. B* **94**, 245132 (2016).

[23] Nobuyuki Kurita, Han-Oh Lee, Yoshi Tokiwa, Corneliu F. Miclea, Eric D. Bauer, Filip Ronning, J. D. Thompson, Zachary Fisk, Pei-Chun Ho, M. Brian Maple, Pinaki Sengupta, Ilya Vekhter, and Roman Movshovich, *Phys. Rev. B* **82**, 174426 (2010).

[24] M. Nicklas, S. Kirchner, R. Borth, R. Gumeniuk, W. Schnelle, H. Rosner, H. Borrmann, A. Leithe-Jasper, Yu. Grin, and F. Steglich, *Phys. Rev. Lett.*, **109**, 236405 (2012).

[25] Binod K. Rai, Macy Stavinoha, Jacintha Banda, C.-L. Huang, M. Brando, and E. Morosan, *in preparation*.

[26] B. Chabot, N. Engel, and E. Parthé, *Acta Crystallogr.*, **B37**, 671 (1981).

[27] P. Lorenz, and W. Jung, *Acta Cryst.* **E62**, i173 (2006).

[28] Macy Stavinoha, C.-L. Huang, and E. Morosan, *in preparation*.

[29] Dongjin Jang, Thomas Gruner, Alexander Steppke, Keisuke Mitsumoto, Christoph Geibel, and Manuel Brando, *Nat. Commun.* **6**, 8680 (2015).

[30] M. Nicklas, in: Strongly Correlated Systems Experimental Techniques, edited by A. Avella and F. Mancini, Springer Series in Solid-State Sciences, Vol. 180 (Springer, Berlin, Heidelberg, 2015), pp. 173204.

[31] G. Cordier, and Ch. Dietrich, *Zeitschrift für Kristallographie - Crystalline Materials.*, **211**,118 (1996).

[32] Yuriy Verbovytskyy, *Chem. Met. Alloys* **7**, 42 (2014).

[33] S. E. Latturner, D. Bilc, J. R. Ireland, C. R. Kannewurf, S. D. Mahanti, and M. G. Kanatzidis, *J. Solid State Chem.* **170**, 48 (2003).

[34] M. Falmbigl, F. Kneidinger, A. Grytsiv, H. Michor, H. Müller, P. Rogl, E. Bauer, G. Hilscher, G. Giester, *Intermetallics* **42**, 45 (2013).

[35] J. P. Remeika, G. P. Espinosa, A. S. Cooper, H. Barz, J. M. Rowell, D. B. McWhan, J. M. Vandenberg, D. E. Moncton, Z. Fisk, L. D. Woolf, H. C. Hamaker, M. B. Maple, G. Shirane, and W. Thomlinso, *Solid State Comm.* **34**, 923 (1980).

[36] Binod K. Rai, Iain W. H. Oswald, J. K. Wang, G. T. McCandless, J. Y. Chan, and E. Morosan, *Chem. Mater.* **27**, 2494 (2015).

[37] Jacintha Banda, Binod K. Rai, E. Morosan, C. Geibel, and M. Brando, arXiv:1806.04983 *submitted to PRB*.

[38] Michael E. Fisher, *Philos. Mag.* **7**, 1731 (1962).

[39] L. J. DE Jongh and A. R. Miedema, *Adv. Phys.* **23**, 1 (1974).

[40] S. Doniach, *Physica* **91B**, 231 (1977).

[41] G.-F. von Blanckenhagen and G.R. Stewart, *Solid State Commun.* **108**, 535 (1998)

[42] R. Kraft, R. Pöttgen, and D. Kaczorowski, *Chem. Mater.* **15**, 2998 (2003)

[43] B. M. Mhlungu and A. M. Strydom, *Physica B* **403**, 862 (2008)

[44] M. O. Ajeesh, T. Shang, W. B. Jiang, W. Xie, R. D. dos Reis, M. Smidman, C. Geibel, H. Q. Yuan, and M. Nicklas, *Sci. Rep.* **7**, 7338 (2017)

[45] C. L. Huang, V. Fritsch, B. Pilawa, C. C. Yang, M. Merz, and H. v. Löhneysen, *Phys. Rev. B* **91**, 144413 (2015)

[46] M. Lenkewitz, S. Corsépius, and G.R. Stewart, *J. Alloys Compd.*, **241**, 121 (1996)

[47] A. Grytsiv, E. Bauer, St. Berger, G. Hilscher, H. Michor, Ch. Paul, P. Rogl, A. Daoud-Aladine, L. Keller, T. Roisnel, and H. Noel, *J. Phys: Condens. Matter* **15**, 3053 (2003)

[48] D. Gignoux, D. Schmitt, and M. Zerguine, *Solid State Commun.* **58**, 559 (1986)

[49] Y. Oner, O. Kamer, Joseph H. Ross Jr., C.S. Lue, and Y.K. Kuo, *Solid State Commun.* **136**, 533 (2005)

[50] C. L. Huang, V. Fritsch, W. Kittler, and H. v. Löhneysen, *Phys. Rev. B* **86**, 214401 (2012)

[51] M. Klicpera, S. Mašková, M. Diviš, P. Javorský, and L. Havela, *J Magn. Magn. Mater.* **404**, 250 (2016)

[52] A. Loidl, K. Knorr, G. Knopp, A. Krimmel, R. Caspary, A. Böhm, G. Sparn, C. Geibel, F. Steglich, and A. P. Murani, *Phys. Rev. B* **46**, 9341 (1992)

[53] Yongkang Luo, Jinke Bao, Chenyi Shen, Jieke Han, Xiaojun Yang, Chen Lv, Yuke Li, Wenhe Jiao, Bingqi Si, Chunmu Feng, Jianhui Dai, Guanghan Cao, and Zhu-an Xu, *Phys. Rev. B*, **86** 245130 (2012)

[54] H. Nakotte, E. Brück, K. Prokes, J.H.V.J. Brabers, F.R. de Boer, L. Havela, K.H.J. Buschow, and Yang Fu-ming, *J. Alloys Compd.* 207/208, **245** (1994)

[55] K. Shigetoh, A. Ishida, Y. Ayabe, T. Onimaru, K. Umeo, Y. Muro, K. Motoya, M. Sera, and T. Takabatake, *Phys. Rev. B* **76**, 184429 (2007)

[56] R. E. Baumbach, T. Shang, M. Torrez, F. Ronning, J. D. Thompson, and E. D. Bauer, *J. Phys.: Condens. Matter* **24**, 185702 (2012)

[57] Leslie M. Schoop, Andreas Topp, Judith Lippmann, Fabio Orlandi, Lukas Müchler, Maia G. Vergniory, Yan Sun, Andreas W. Rost, Viola Duppel, Maxim Krivenkov, Shweta Sheoran, Pascal Manuel, Andrei Varykhalov, Binghai Yan, Reinhard K. Kremer, Christian R. Ast, and Bettina V. Lotsch *Sci. Adv.* **4**, eaar2317 (2018).

[58] S. A. Shaheen, *J. Appl. Phys.* **63**, 3411 (1988)

[59] A. Thamizhavel, R. Kulkarni, and S. K. Dhar, *Phys. Rev. B* **75**, 144426 (2007)

[60] J.G. Sereni, P. Pedrazzini, M. Gómez Berisso, A. Chacoma, S. Encina, T. Gruner, N. Caroca-Canales, and C. Geibel, *J. Phys.: Conf. Ser.* **592**, 012005 (2015)

[61] Surjeet Singh, S.K. Dhar, P. Manfrinetti, and A. Palenzona *J. Alloys Compd.* **298**, 68 (2000).

[62] B D White, D Yazici, P-C Ho, N Kanchanavatee, N Pouse, Y Fang, A J Breindel, A J Friedman and M B Maple, *J. Phys.: Condens. Matter* **27**, 315602 (2015).

[63] G. M. Sheldrick, SHELX-2013-Programs for Crystal Structure Analysis: i. Structure Determination (SHELXS) and ii. Refinement (SHELXL-2013), University of Gottingen, Germany (2013).

[64] G. M. Sheldrick, SHELXT Integrated space-group and crystal-structure determination, *Acta Crystallogr., Sect. A* **71**, 3 (2015).

Appendix

Room temperature powder patterns were collected using a Bruker D8 x-ray diffractometer using Cu Kα radiation. The x-ray patterns were refined using TOPAS software. For single crystal x-ray refinement, fragments of $CeIr_3Ge_7$ were obtained by cutting larger crystals to an appropriate size. These fragments were mounted onto glass fibers using epoxy and then mounted onto a Bruker D8 Quest Kappa single crystal x-ray diffractometer equipped with an IμS microfocus source (λ = 0.71073 Å) operating at 50 kV and 1 mA, a HELIOS optics monochromator, and a CMOS detector. The collected data were corrected for absorption using the Bruker program SADABS (multi-scan method). The crystal structure of $CeIr_3Ge_7$ was solved using direct methods in SHELXS2013[63] and all atomic sites were refined anisotropically using SHELXL2014[64]. The orientation along the a and c axes in the hexagonal setting of $CeIr_3Ge_7$ single crystals were determined by the backscattering x-ray Laue method.

TABLE I: Crystallographic parameters of $CeIr_3Ge_7$ single crystals at T = 298 K ($R\bar{3}c$)

a (Å)	7.8915(8)
c (Å)	20.788(6)
V (Å^3)	1121.1(4)
crystal dimensions (mm^3)	0.02 x 0.04 x 0.06
θ range ($^\circ$)	5.2 - 30.3
extinction coefficient	0.00102(7)
absorption coefficient (mm^{-1})	86.73
measured reflections	7121
independent reflections	384
R_{int}	0.082
goodness-of-fit on F^2	1.18
$R_1(F)$ for ${F^2}_o > 2\sigma({F^2}_o)^a$	0.032
$wR_2({F^2}_o)^b$	0.074

$^a R_1 = \sum \mid\mid F_o \mid - \mid F_c \mid\mid / \sum \mid F_o \mid$

$^b wR_2 = [\sum[w({F_o}^2 - {F_c}^2)^2] / \sum[w({F_o}^2)^2]]^{1/2}$

TABLE II: Non-Kondo Ce compounds. Symbols represent the legend used for Fig. 4(b).

Compound	Symbol	$T_{N/C}$ (K)	AFM/FM	Ce-Ce Bond Distance (Å)	Reference
Ce_3Pt_4	◆	2.8	AFM	3.514	41
CeMgGa	◒	3.1	AFM	3.897	42
CeAuGe	⬓	10.9	FM	3.968	43
$CePd_2As_2$	◆	14.7	AFM	4.268	44
CeAuSn	▶	4.4	AFM	3.858	45, 46
CeAgSn	◀	6.45	AFM	3.855	46
$Ce_2Zn_6Ge_3$	◆	7.2	AFM	4.116	47
CeCuSi	⬒	15.5	FM	3.977	48
CeCuGe	◑	10	FM	3.945	49
$CeAu_2Ge_2$	◧	14.5	AFM	4.367	50
Ce_2Pd_2In	◭	4.5	AFM	4.075	51
$CeRu_2Ge_2$	▼	8.7	FM	4.256	52
$CeNi_2As_2$	◓	4.8	AFM	4.081	53
CeCuSn	◐	8.6	AFM	3.924	54
$CeRh_3B_2$	□	115	FM	3.096	17, 18
$CeIr_3Si_2$	◆	4.1	AFM	3.607	55
$CeRu_2Ga_2B$	◨	16.3	FM	4.187	56
CeSbTe	▲	2.75	AFM	4.37	57
CeSi	▼	5.6	AFM	3.76	58
$CeAg_2Ge_2$	▲	4.6	AFM	4.301	59
CeScGe	▲	47	AFM	3.864	60
$Ce_3Cu_4Si_4$	▶	10.4	AFM	3.922	61
$Ce_3Pt_{23}Si_{11}$	○	0.44	FM	5.95	19, 20
$CeIr_3Ge_7$	★	0.63	AFM	5.724	current work